CLIMATOLOGY

Little Ice Age abruptly triggered by intrusion of Atlantic waters into the Nordic Seas

Francois Lapointe* and Raymond S. Bradley

The Little Ice Age (LIA) was one of the coldest periods of the postglacial period in the Northern Hemisphere. Although there is increasing evidence that this time interval was associated with weakening of the subpolar gyre (SPG), the sequence of events that led to its weakened state has yet to be explained. Here, we show that the LIA was preceded by an exceptional intrusion of warm Atlantic water into the Nordic Seas in the late 1300s. The intrusion was a consequence of persistent atmospheric blocking over the North Atlantic, linked to unusually high solar activity. The warmer water led to the breakup of sea ice and calving of tidewater glaciers; weakening of the blocking anomaly in the late 1300s allowed the large volume of ice that had accumulated to be exported into the North Atlantic. This led to a weakening of the SPG, setting the stage for the subsequent LIA.

INTRODUCTION

The Little Ice Age (LIA) was the coldest period in the Holocene in the Northern Hemisphere (NH). It began in the 13th century because of a drop in temperatures (following the eruption of Samalas in 1257 CE), but temperatures fell abruptly again in the early 15th century (*1*). There is evidence that this period was caused by increased Arctic sea ice export that led to cooling in the North Atlantic (*2*, *3*). Several studies have argued that this cooling anomaly resulted in reduced meridional heat transport by the Atlantic Meridional Overturning Circulation (AMOC) (*4*–*6*), although this hypothesis is not supported by a recent reconstruction of AMOC strength (*7*) or by transient model simulations (*2*). The AMOC has only been directly monitored since 2004, and understanding of its long-term variability is limited (*8*). In contrast, the Atlantic multidecadal variability (AMV), a basin-wide index of sea surface temperature (SST) variability in the North Atlantic, is based on more than a century of instrumental data (*6*). A hot spot of AMV changes is located on the subpolar gyre (SPG) (*9*), and so, proxy records that track SSTs from this area are very valuable to better understand the long-term AMV evolution. The SPG's influence on the North Atlantic and the Arctic Ocean is an important feature of the climate system as it modulates the transport of heat in the Labrador and Nordic Seas both in the preindustrial and the anthropogenic era (*10*).

In fully coupled climate models with strong AMOC variability, the presence of a basin-wide horseshoe-shaped warming pattern over the North Atlantic is consistent with the observed positive phase of the AMV (*11*, *12*), with warming in the subpolar North Atlantic (SPG) and cooling in the Gulf Stream region (Fig. 1) (*9*, *11*, *13*). During the negative phase of the AMV, the opposite pattern prevails. Hence, investigating how this dipole AMV fingerprint changed during the transition from Late Medieval time into the LIA may provide insights into the state of the AMOC, and associated teleconnections, during that period.

In recent years, an increasing number of marine records with subdecadal temporal resolution—sufficient enough to detect abrupt changes in the overturning circulation—have been reported (*7*, *14*). These records are crucial to understand the long-term evolution of the AMV (AMOC) and whether it underwent rapid changes in strength. In a recent study, a period of extreme sea ice export in the mid to late 14th century was documented and linked to the coldest conditions in the North Atlantic that occurred in the 1400s (*15*). This export of sea ice is thought to have triggered the shutdown of deep convection in the SPG (*16*–*18*). Furthermore, a strong weakening of

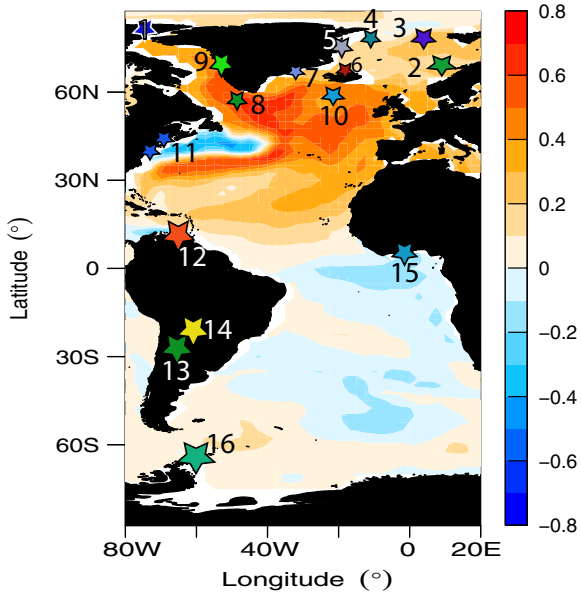

Fig. 1. AMOC SST fingerprint. Multimodel mean correlation map between the low-frequency AMOC at 26°N and SST (*12*). Stars numbered 1 to 16 denote location of sites referred in the figures. The reconstructed AMV at South Sawtooth Lake (*1*), August temperature in Vøring Plateau off Norway (*2*), Eastern Fram Strait IRD (*3*), Atlantic water influence based on *C. neoteresis* in Western Fram Strait (*4*), East Greenland Strait *N. labradorica* (*5*), North Icelandic shelf temperature based on $\delta^{18}O$ from bivalve shells (*6*), IRD in Denmark Strait (*7*), the RAPiD-35-COM $\delta^{18}O$ *T. quinqueloba* (*8*), percentage of Atlantic species in Disko Bugt (*9*), the RAPID-21-COM sortable silt in the ISOW (*10*), Gulf of Maine reconstructed SST from bivalve shells (*11*), titanium (%) in the Cariaco Basin (*12*), Quelccaya ice record $\delta^{18}O$ (*13*), Huagapo speleothem $\delta^{18}O$ (*14*), and Lake Bosumtwi lake level inferred from $\delta^{18}O$ (*15*). The James Ross Island ice core record with annually resolved δD is shown (*16*).

Department of Geosciences, Climate System Research Center, University of Massachusetts Amherst, Amherst, MA, USA.
*Corresponding author. Email: flapointe@umass.edu

the AMOC may be linked to a southward shift of the intertropical convergence zone (ITCZ), as seen in numerous models (*19*, *20*) and in paleoclimatic records across a range of time scales (*21*, *22*), implying linkages between the AMV, AMOC, and ITCZ over the past millennium (*6*, *20*). Here, using highly resolved records (mostly subdecadal) from key sites, we provide multiple lines of evidence that warm Atlantic water intrusion into the Nordic Seas occurred in the 1300s, and this positive AMV anomaly played a key role in the weakening of the SPG strength leading to a decline of the AMOC in the early 1400s, followed by intensive cooling. We ascribe the unusual 14th century intrusion of warm water to an exceptional period of North Atlantic blocking that led to enhanced warm water advection into the Nordic Seas.

RESULTS

North Atlantic Current north of 55°N.

Reconstructed Atlantic SSTs show an anomalously cold period from ~1400 to 1620 CE, which is unique in the context of the past ~3 millennia (*23*). Before this abrupt temperature decline, the AMV shows a double warm peak in the 14th century, around 1320 and 1380 CE, and a trough in the mid 1300s, a pattern remarkably similar with another well-dated reconstructed AMV record (*24*). In the Vøring Plateau off Norway, a diatom-based SST reconstruction highlights warmer conditions through the late 1300s (Fig. 2A). This marine record is highly resolved (2 to 17 years, subdecadal on average) and located under the direct influence of the Norwegian Atlantic Current, a poleward extension of the Gulf Stream where warm and saline Atlantic water enters the Arctic (*25*). There is significant covariability between AMV and this proxy (past 1000, $r = 0.29$, $P < 0.0001$). SST warming in the late 1300s is also reflected in the foraminifera *Neogloboquadrina pachyderma* (dextral and sinistral) from the Vøring Plateau (fig. S1) (*26*), indicating that this warming was not simply confined to summer months. Fourteenth century warming is also expressed in a high-resolution marine record off western Svalbard (*27*), in eastern Fram Strait: Two maxima in ice rafted debris (IRD) were in phase with the two warm peaks of the reconstructed AMV (Fig. 2B) (*23*). These higher amounts of IRDs are related to increasing iceberg/sea ice abundance originating from western Svalbard and may be the result of calving induced by the warmer SSTs (*28*). In Northeast Greenland (western Fram Strait), two prominent peaks of lower $\delta^{18}O$ from *Cassidulina neoteretis* are in phase with the warm peaks found in the AMV (Fig. 2C). Low *Cassidulina neoteretis* $\delta^{18}O$ indicates high calcification temperature that is linked to the inflow of Atlantic water (*29*). We also note that a warm peak at ~1000 CE also coincided with higher Atlantic SSTs (Fig. 2C). Similarly, in a highly resolved (<20 years) marine record off the central Greenland shelf (at 73°N), the strongest increase in *Nonionellina labradorica* in the past ~1500 years was also in the late 1300s (Fig. 2D). This species is diagnostic of productive intermediate Atlantic waters, i.e., the water associated with a strengthening of the East Greenland Current (EGC) (*30*, *31*). Without any chronological adjustments, the coherence between the east Fram Strait IRD record and variations in *N. labradorica* over the past ~700 years is especially notable ($r = 0.62$; fig. S2 and Supplementary Text). Further downstream around the Denmark Strait, IRD reaches its highest Holocene values at ~1380 CE (Fig. 2D) (*32*).

Before the 20th century, the greatest positive SST anomaly in an annually resolved marine oxygen isotope from the North Icelandic shelf was also at ~1350 to 1380 (Fig. 3A) (*33*). A similar pattern is also recorded by $\delta^{18}O$ in the DYE-3 ice core record (*23*). Because of its southern location on Greenland, the DYE-3 ice record is sensitive to North Atlantic warming (*23*). Uncertainties in the chronology of these marine records may be associated with temporal offset among them; however, they all have chronological tie points in the period of interest. In addition, the fact that they exhibit two peaks at the end of the 1300s suggests a contemporaneous climatic event (Supplementary Text). Collectively, these records all point to an anomalously strong poleward flux of heat into the northeastern North Atlantic in the late 1300s extending as far north as the West Spitsbergen Current (*27*) with a concomitant strengthening of the EGC (Fig. 2, A to D).

Strong volcanic eruptions in the mid 1200s resulted in increased sea ice extent and glacier growth in the Arctic (*34*, *35*). Hence, exceptionally extensive and thick Arctic sea ice characterized the beginning of the LIA in the mid to late 1200s, and so, an Atlantic Water intrusion would have had a significant calving impact, similar to conditions reported in modern times (*36*). The fact that the reconstructed AMV is in phase with increased IRD and many Atlantic SST–related proxies from the Nordic Seas point to an extreme calving event around 1380 CE that triggered what seems to be one of the most extreme calving events in millennia (Fig. 2D) (*15*). Although there is no direct evidence of the sea ice conditions off Svalbard at that time, we speculate that the late 1300s was a period of massive calving and export of sea ice caused by the returning Atlantic waters.

The availability of highly resolved proxies from the Labrador Sea also enables an investigation of the anomalies seen in the late 1300s in the downstream path of the EGC. $\delta^{18}O$ in planktonic foraminifera (*N. pachyderma*), a proxy for near-surface water properties, shows low values during the interval ~1320 to 1380, indicating a reduction in polar water in the Labrador Sea (Fig. 3B) (*14*, *18*). This is further corroborated by a shift to lower $\delta^{18}O$ of *Turborotalita quinqueloba*, indicative of warmer SST conditions (*18*). This indicates the increased presence of relatively warm and salty Atlantic waters in this area (*14*), in line with the reconstructed Atlantic SSTs (Fig. 3, B and C). We note that this relationship (between subpolar salinity from 0 to 1500 m in the SPG and the AMV) is clearly seen in the instrumental period (fig. S3).

There is also evidence for warmer SSTs in western Greenland at the end of the 14th century. The percentage of warm Atlantic water indicators at Disko Bugt abruptly increased around 1380 CE, including *Melonis barleeanus*, an Atlantic water species, which reached unprecedented abundance during this period (Fig. 3D) (*37*). Together, the coherent spatiotemporal increase in all these highly resolved records across a vast swath of the North Atlantic highlights that the AMV (warm Atlantic SSTs) was a critical precursor to the extreme ice anomaly of the late 14th century (*15*).

AMOC fingerprint during the transition from the late 1300s to the 1400s

A new sortable silt record from the Iceland-Scotland Overturning Water (ISOW) region (*14*) has an extremely high temporal resolution (~6 years) throughout the past 3000 years. A notable feature of this record is the period 1400–1620 CE, which shows the strongest increase in ISOW concomitant with an abrupt decrease in SSTs. Strong ISOW flow speeds are interpreted as resulting from a reduction in Labrador Sea Water in the Icelandic Basin, associated with weaker deepwater formation in the Labrador Sea (*14*). This abrupt

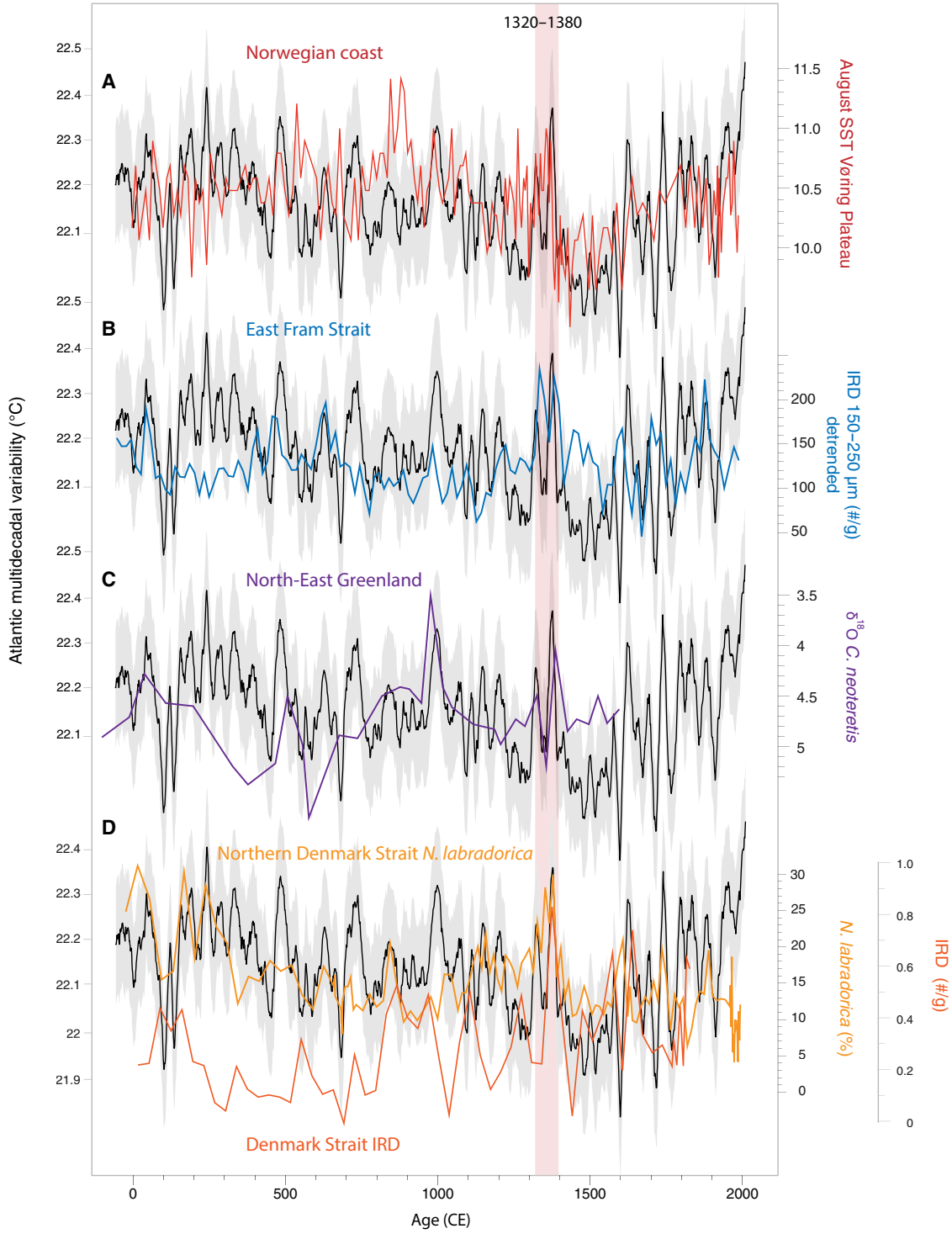

Fig. 2. Upstream and downstream path of the North Atlantic Current in the Arctic. (**A**) Reconstructed August temperature in the Vøring Plateau (*25*), compared to AMV. (**B**) High-resolution IRD on the Eastern Fram Strait [core MSM5/5-712 (*28*)]. The IRD data were detrended to remove the neoglacial cooling trend. (**C**) *C. neoteretis*, a proxy for warm Atlantic waters in Western Fram Strait (core PS93/025) (*29*). (**D**) *N. labradorica*, a proxy for chilled Atlantic waters from core PS2641-4 (*30*) and IRD reported in Denmark Strait (*32*). The AMV is filtered by a 21-year Gaussian filter, and the gray-shaded area is the 95% confidence level of the reconstruction (*23*).

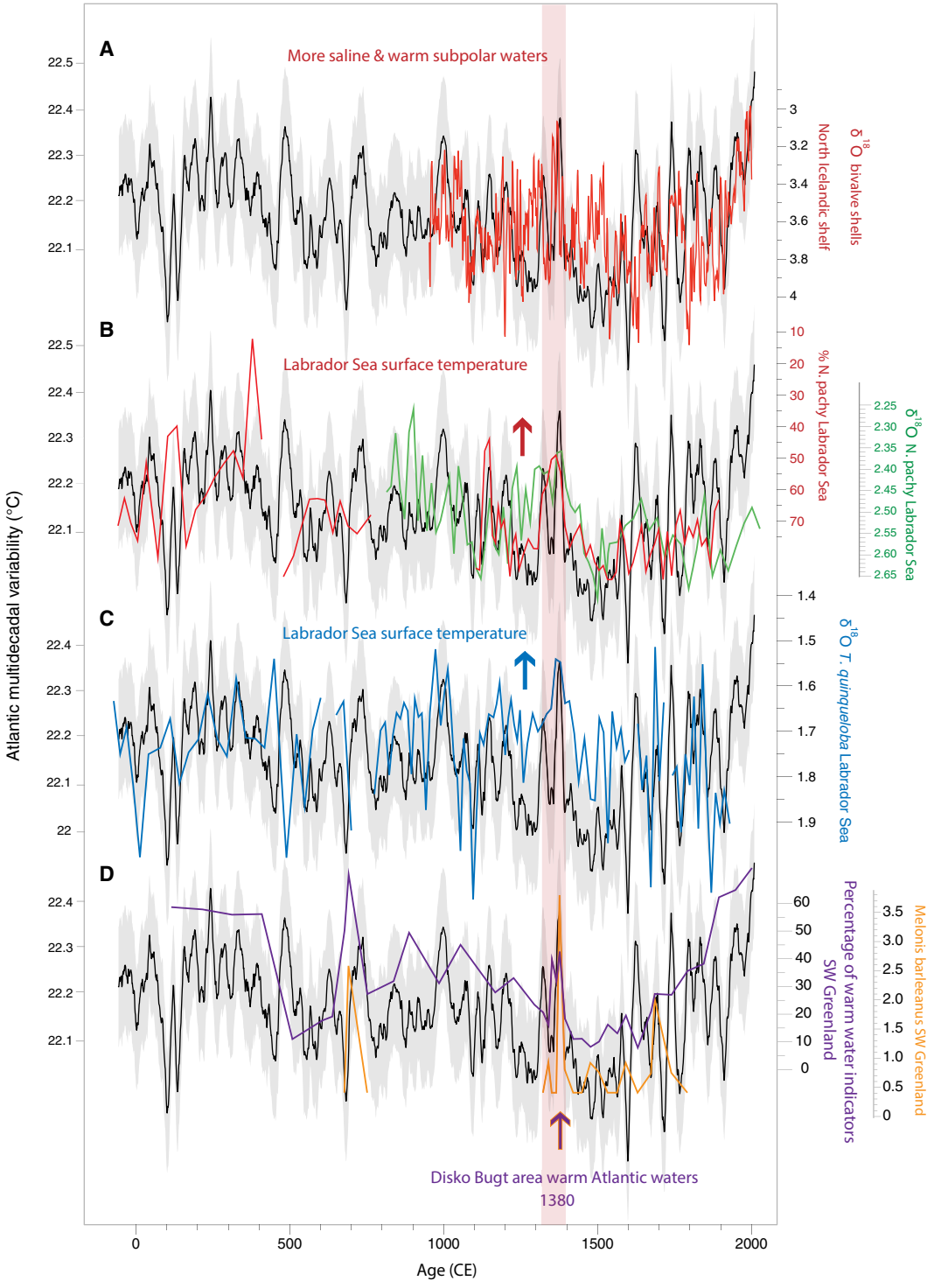

Fig. 3. SPG SST anomalies in the past ~2000 years. (**A**) $\delta^{18}O$ of bivalve shells in the Iceland basin (*33*) shelf compared to the AMV. (**B**) Sea surface conditions in the Labrador Sea from $\delta^{18}O$ in *N. pachyderma* (red) in site RAPiD-35-COM (*14*) and green (*18*). (**C**) *T. quinqueloba* $\delta^{18}O$ from site RAPiD-35-25B at Eirik Drift (*18*). (**D**) Percentage of warm water indicators at Disko Bugt, South West (SW) Greenland with the individual Atlantic species *Melonis barleanus* (*37*).

anomaly, which occurred within two decades, is unprecedented in the past ~3000 years. It indicates that higher ISOW flow speeds were associated with lower Atlantic SSTs, consistent with the notion of weak deepwater formation (a contracted SPG) in the Labrador Sea during the coldest interval of the LIA that started in the 1400s (Fig. 4A). A recent reconstruction of AMOC (*7*) covaries generally well with the AMV (Fig. 4B and fig. S4), as revealed by a significant negative correlation ($r = -0.26$, $P < 0.001$; annual). The reconstructed

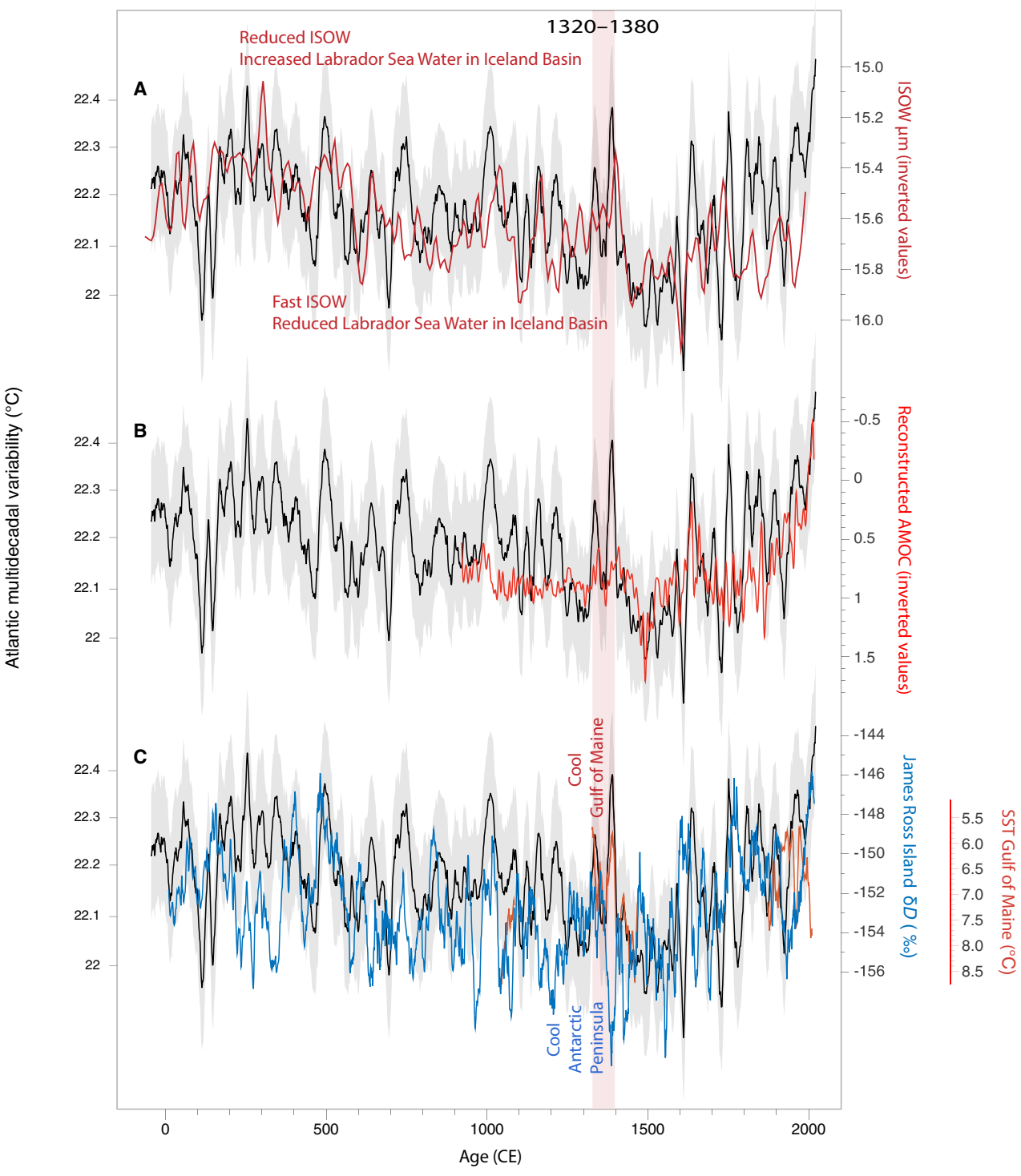

Fig. 4. AMOC fingerprint during the transition from the 14th to the 15th century. (**A**) Iceland-Scotland Overturning Water (ISOW) sortable silt (*14*) compared to reconstructed AMV. (**B** and **C**) Same as in (A), but for reconstructed AMOC (*7*) and (C) for the reconstructed SST in the Gulf of Maine from bivalve shells (red) (*38*). The blue curve in (C) is the annually resolved δ*D* record from James Ross Island, Antarctica. The ISOW record is filtered by a 3-point Gaussian filter (A), and the bivalve shell record is smoothed by a 5-year Gaussian filter (C) and the James Ross Island temperature record. ‰, per mil.

AMOC index is based on the difference between the SPG and the NH temperature, and so it is reasonable to expect that these proxies exhibit similar variability because our record is itself correlated with SPG SSTs (Fig. 3 and fig. S3) (*23*). Of note is the very strong AMOC during the early phase of LIA (~1400 to 1600 CE), with greatest values in the mid 1400s (Fig. 4B), which is at odds with the general view that a weakened AMOC prevailed during the LIA. However, because this AMOC index is based on the difference between the SPG and the NH temperature, higher values of this index would be expected as the NH temperature is known to have been much colder during the LIA. Thus, investigating other key hot spots of the AMOC fingerprint may help to better resolve conditions during the LIA and the transition in the 14th to the 15th century.

There are few highly resolved records of past SSTs from the U.S. east coast, but one reconstruction overlaps the period of the late 1300s. The coolest period recorded in a unique annually resolved SST record from the Gulf of Maine (*38*) is in phase with the strong positive AMV of the late 1300s (Fig. 4B), indicating a dipole SST anomaly between the SPG and the U.S. East Coast, diagnostic of a strong AMOC (Fig. 1). Conversely, weakened deepwater formation during the 1400s resulted in the opposite dipole pattern of SSTs, with warmer conditions in the Gulf Stream region (U.S. East Coast) and cooler SSTs in the North Atlantic (SPG) (Fig. 4C). This is a feature also seen in reconstructed SST from Chesapeake Bay on the U.S. East Coast (fig. S5) (*39*).

Late 14th century climate anomaly as expressed from tropical proxy records

Studies of instrumental data, model simulations, and paleoclimatic records over a wide range of time scales have shown that a reduction in AMOC strength leads to a rapid atmospheric response, most notably in the southward displacement of the ITCZ and associated convective rainfall (*5*, *6*, *20*, *22*). Accordingly, southward migration of the ITCZ during the LIA has been documented in Asia (*40*, *41*), Africa (*42*), South America (*43*, *44*), Central America (*21*), and North America (*45*). In the Pacific, the southward migration of the ITCZ during the LIA period was preceded by a more northerly ITCZ in the late 1300s (*44*), as shown by lower (higher) δD values of lipids in the tropical central Pacific (Washington Lake at 5°N), which details wetter (drier) conditions that closely match the AMV (Fig. 5A). To investigate further whether past AMV changes were linked to shifts in the ITCZ, we examined subdecadally resolved proxy records from tropical regions known to be sensitive to variations in the ITCZ. Increased titanium in Cariaco Basin sediments throughout the 14th century is associated with enhanced precipitation over the Orinoco Basin, indicating times when the ITCZ position shifted north (fig. S6) (*43*). In addition, planktic foraminifer *Globigerina bulloides* abundance in the Cariaco Basin, a proxy for upwelling intensity, decreased (increased) sharply in the late 1300s (early 1400s) in close agreement with the reconstructed AMV (*23*). This is coherent with weakened (strengthened) trade winds during periods of warming (cooling) of the North Atlantic and associated shifts in the ITCZ (*20*). This is further supported by strong positive excursions of $\delta^{18}O$ in the extremely well-dated Huagapo Cave speleothem (*46*) and Quelccaya ice core records (*47*), all suggestive of drier conditions in Peru (Fig. 5B and fig. S6). The annually resolved Quelccaya ice record also reveals that the end of the 1300s was characterized by the lowest ice accumulation of the past thousand years (Fig. 5C).

In Western Africa, authigenic carbonate $\delta^{18}O$ in Lake Bosumtwi is associated with the balance between precipitation and evaporation (*48*). As the lake is a closed basin, the lower $\delta^{18}O$ is indicative of a higher lake level and vice versa (*48*). Reconstructions highlight that periods of high precipitation are associated with periods of positive AMV (*48*), in line with observations and climate model simulation (*6*). A salient feature of the record from Lake Bosumtwi is the abrupt increase in lake level (decrease in $\delta^{18}O$) that occurred in the late 14th century, consistent with what would be expected from a positive AMV (Fig. 5D). The return to drier lake conditions during the LIA (increased $\delta^{18}O$) from ~1400 to 1615 corresponds to cooler SSTs in the North Atlantic. The synchronicity among these proxies and particularly the in-phase double peak seen in the 14th century is remarkable given the distance and suggests a more northerly ITCZ in the late 1300s, followed by a southward displacement in the early 1400s (Fig. 5 and fig. S6) as expected from model simulations of the climatic response in the Tropics to a slowdown in AMOC.

DISCUSSION

There are few studies that have investigated the role of Atlantic water on the EGC strength; however, recent monitoring indicates that the returning Atlantic Current is a key component of the EGC. Observational and model evidence show that the evolution of the barotropic Arctic Ocean outflow to the baroclinic conditions of the EGC is modulated by the recirculation of Atlantic water in the Fram Strait (*49*). As the north Atlantic waters reach closer to the east Greenland shelf break, the Arctic Ocean outflow becomes restricted to an increasingly narrow band along the shelf break, causing the EGC to gain velocity. Hence, this is indicative that both the Arctic Ocean water and Atlantic returning water combine to form the EGC (*49*). Several observational studies have also shown that the Atlantic recirculation extends to 78°N and can reach as far as or beyond 81°N (*49*, *50*). On the basis of the paleo evidence shown in this study (Figs. 2 and 3), the late 1300s was a period of strengthened North Atlantic Current that resulted in strong Atlantic recirculation in the Fram Strait region that enhanced the EGC strength. A coupled climate model simulation, with an improved representation of the Gulf Stream extension, shows that increased melting of Arctic sea ice is strengthened by an inflow of warm Atlantic waters, which characterizes the positive phase of the AMV (*51*). In both models and observations, the EGC is then pivotal in driving the southward transport of sea ice. It takes ~20 years after the maximum positive AMV to weaken the deep convection and terminate the AMV warm phase (*51*). This result is in agreement with the two decades that elapsed between ~1380 (maximum positive AMV) and an abrupt decline of Arctic sea ice in Fram Strait, with a strong increase in sea ice in the downstream region (EGC through West Greenland Current) culminating in the 1400s (*15*).

It has been established that positive phases of the AMV, i.e., a warmer and more saline subpolar Atlantic ocean, result in more persistent atmospheric blocking over the North Atlantic (80°N–30°N, 50°W–40°E) (*52*). A comparison of monthly reconstructed Greenland/European 500-hPa geopotential height (80°N, 30°N–50°W, 40°E) with the reconstructed AMV shows strong covariability, indicating that the reconstructed AMV captures these blocking events (Fig. 6A). There is a strong increasing trend in the 500-hPa geopotential height from ~1980 to the present, in line with a weakened polar jet stream over the North Atlantic region and increasing atmospheric blocking events. These modern linkages imply that the strong and sustained positive AMV around 1380 CE was also a period of enhanced

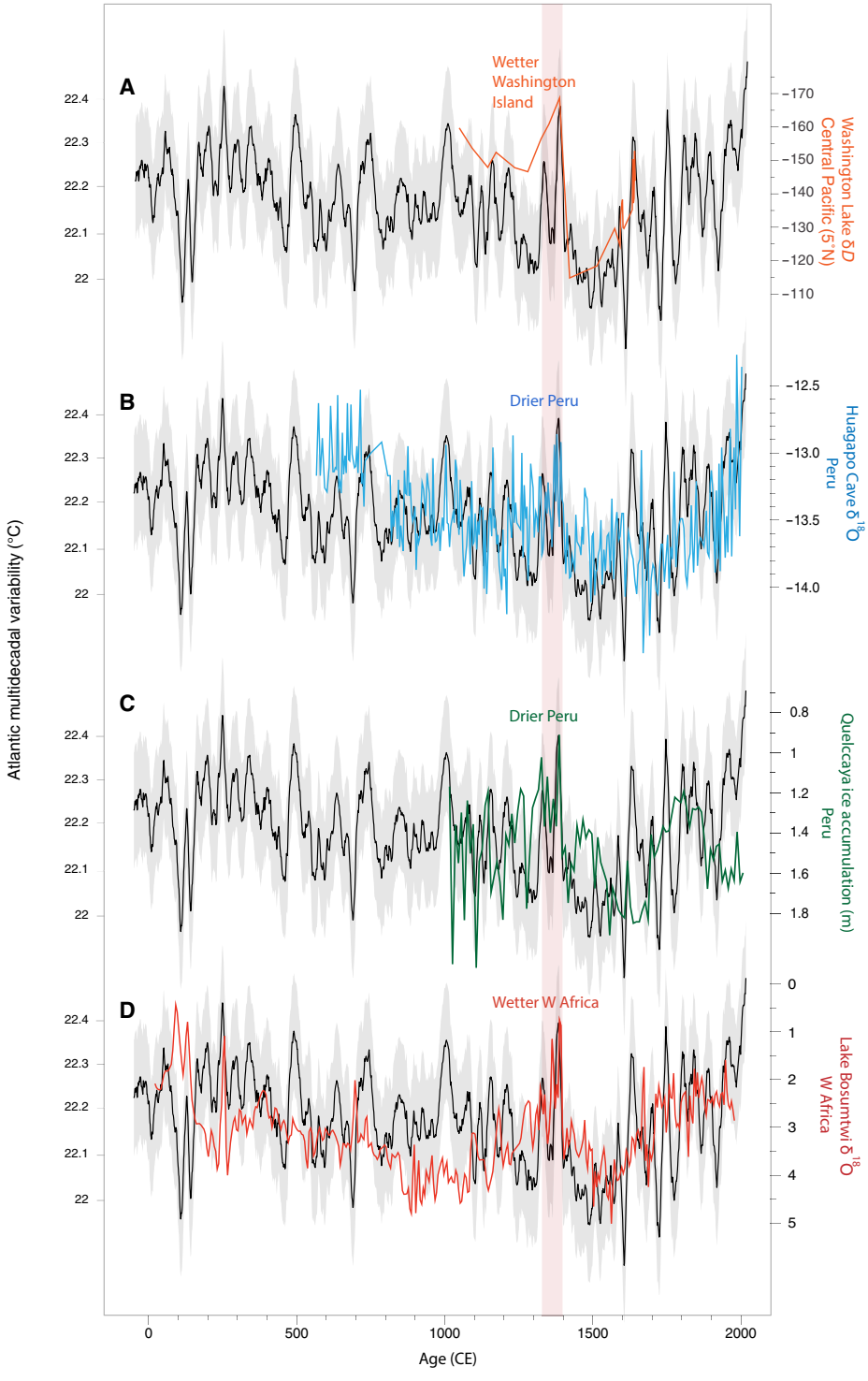

Fig. 5. Expression of the late-1300s climate anomaly from tropical proxy records. (**A**) δD at Washington Lake, Central Pacific (*44*); (**B**) Huagapo Cave $\delta^{18}O$ in Peru (*46*); (**C**) ice accumulation in meters at Quelccaya Ice Cap, Peru (*47*); and (**D**) $\delta^{18}O$ at Lake Bosumtwi (*48*) in Western (W) Africa.

blocking as shown by warmer SSTs in the SPG and Nordic Seas (Figs. 2 and 3). After 1380 CE, with a reduction in blocking and a weakening of the influx of warm saline water into the Nordic Seas, a flushout of Arctic sea ice through Fram Strait occurred, reaching a peak in the 1400s (*15*). We propose that atmospheric blocking over the North Atlantic led to a warmer and more saline subpolar Atlantic Ocean, i.e., the positive AMV phase, and a subsequent increase in sea ice export via the EGC (*53*–*56*). Recent conditions offer an analogy to this situation. The strongest blocking episode of the past five decades [1960 to 1965; figure S8 in (*52*)] promoted the accumulation

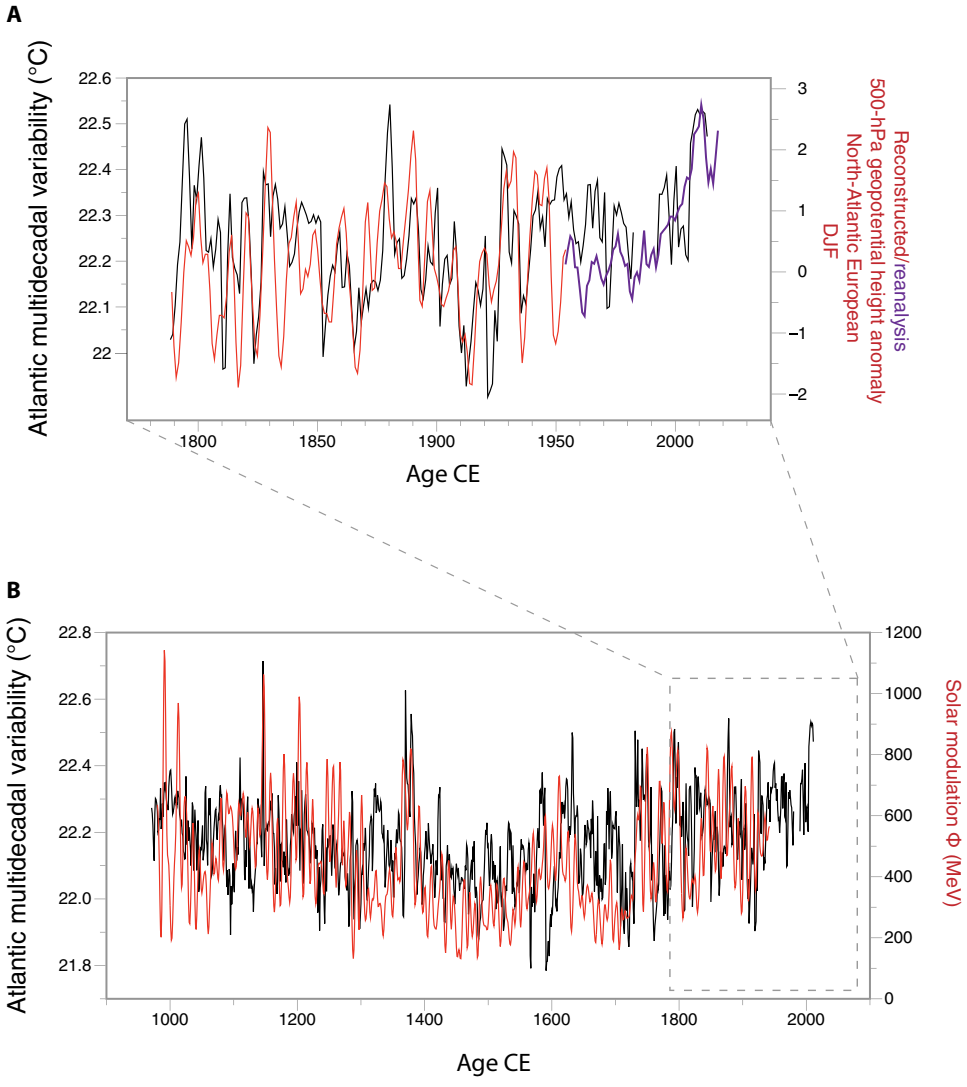

Fig. 6. AMV, Atlantic blocking, and solar forcing. (**A**) The winter (December to February) North-Atlantic/European atmospheric pattern as seen in the reconstructed 500-hPa geopotential height in the region 80°N–30°N, 50°W–40°E (*81*) compared to the reconstructed annual AMV. In purple is the 500-hPa geopotential height from the 20th century reanalysis V3 (*82*) from 1950 to 2015. (**B**) Reconstructed annual solar modulation parameter (red) (*65*) with reconstructed annual AMV. The solar activity reconstruction is shifted 7 years toward present (increasing correlation occurs between −2 lag and +11 years, solar leads, $r = 0.31$, $P < 0.0001$). The 500-hPa geopotential height anomalies are filtered by a 5-year Gaussian filter to improve visibility.

of Arctic sea ice in the 1960s followed by a flushout in the 1970s that contributed to a weakened SPG and AMOC few years after (*56*). Reconstructed Arctic sea ice extent reveals low values around ~1400 (*57*). This is in accordance with the removal of Arctic sea ice that culminated in the 1400s, and it suggests that the post–1380 CE reduction in blocking was a key driver of sea ice loss via increased transport in the EGC, seen in both models and paleo data (Fig. 2). This subsequently led to sea ice accumulation downstream in the subpolar region (*15*), while higher latitude Arctic sea ice remained low in the early 1400s (*15*, *51*, *56*).

Variability in winter blocking frequency in the Atlantic/European sector has been linked to the 11-year solar cycle (*58*–*62*). Blocking response to solar activity increases for both high and low solar phases, but with a different spatial pattern (blocking center) for each phase (*61*). Periods of high solar activity (as recorded by ^{14}C in tree rings) are associated with Atlantic blocking episodes located over south Greenland, whereas during lower solar activity, blocking tends to be confined to the eastern Atlantic (*61*–*63*). Periods of persistent atmospheric blocking over Greenland are associated with warmer conditions and increased SST (*64*); hence, the strong solar activity documented in the mid to late 1300s may have promoted more persistent blocking over Greenland that allowed Atlantic SST to reach the SPG and the Nordic sea more readily.

Figure 6B compares the reconstructed AMV with the most recent reconstruction of solar activity that spans the past millennium at (sub)annual temporal resolution (*65*). There is a high covariability between these two datasets, most notably in the mid to late 1300s period of higher solar activity (Fig. 6B). This anomalous period of high solar forcing is consistent with the hypothesis of increased atmospheric blocking over the western North Atlantic and Greenland

(*60*, *61*), leading to increased high-latitude moisture transport and warmer conditions in southern Greenland (Fig. 3) (*63*, *66*).

The existence of an SST dipole, similar to that during the strengthening of the AMOC (Fig. 1), is also a spatial pattern depicted during the North Atlantic atmospheric blocking anomalies of the early 1960s (figs. S8 and S9). A warmer SPG (increased blocking during positive AMV) coincides with cooler SST on the U.S. East Coast, a feature that maximizes at a lag of 6 to 7 years (*64*), coherent with the AMV leads in the paleo record (fig. S7), and the antiphase relationship seen during the 1300-to-1400 transition (Fig. 4B). Although this is based on one individual annually resolved SST in the Gulf of Maine that ends in the late 15th century, a highly resolved SST record in Chesapeake Bay also shows abnormally cooler SSTs during the ~1380s (fig. S5), adding support to our hypothesis. Nonetheless, given the lack of highly resolved SST proxy records from this region, it is unknown whether this dipole SST anomaly was a persistent feature lasting until the 1600s, highlighting the need to collect other annually resolved SST record from this region where the SST fingerprint of the AMOC is strongest (*6*).

Transient simulations of the preindustrial period depict one of the strongest increases in SPG strength between 1350 and 1380 (*67*, *68*) in the past millennium, which is notably contemporaneous with the strong positive AMV. This suggests that high solar forcing in the mid to late 1300s, coincident with low volcanic activity, had a profound impact on regional atmospheric circulation. The increase in the SPG strength during the period ~1350–1380 is accompanied by anomalously high wind stress curl, salinity, and mixed layer depth (late winter) over the SPG (*68*). These simulations also highlight that higher meridional heat transport occurred at 26°N, and meridional stream function averaged between 35°N and 45°N at 1000-m depth, similar to what would be expected from a strengthening of the AMOC.

The decades shortly after the 1600s stand out with the strongest increase in ISOW flow speeds during the coolest AMV conditions (Fig. 4A). In transient simulations of the past millennium, this period coincided with extended and thicker sea ice following the cluster of volcanic eruptions in the 1600s (*68*). This resulted in the reduction of surface heat losses causing more stability in the overlying atmosphere and positive anomalies of winter sea level pressure, especially persistent over the western subpolar North Atlantic. A substantial reduction of the wind stress curl over the subpolar basin is thereby simulated during the 1600s (*68*). The increase in ISOW flow speeds during the 1600s was associated with the SPG west-east density gradient that reached lowest values in this period, consistent with observations and paleo evidence (*14*, *69*).

We note that the AMOC is complex and still poorly understood (*8*, *70*). While some studies show a link between increased cooling of the SPG and a reduction of the AMOC (*4*–*6*), others do not associate a weakened SPG to a declining AMOC (*2*, *68*). Model simulations without greenhouse gas forcing suggest that ocean heat transport to the Arctic is enhanced by AMOC strengthening (*10*), whereas under global warming, heat transport to the Arctic is shown to be intensified even with the weakening of the AMOC (*10*, *67*, *71*, *72*).

Dima and Lohmann (*73*) identified two distinct modes of variability in global SST datasets: one global (associated with the gradual decline of the global thermohaline circulation since ~1930s) and the second due to multidecadal SST changes in the Atlantic i.e., the AMV. The global mode is associated with interhemispherically symmetric warming (or cooling) in both northern and southern oceans and represents a long-term forcing. In contrast, the Atlantic mode is related to rapid SST warming in south Greenland and SST cooling in the Antarctic, reminiscent of a seesaw pattern (*73*, *74*), and is linked with rapid change in the overturning circulation spanning interannual to decadal time scales (*73*). Although there is no highly resolved SST reconstruction in the Southern Ocean to investigate a possible interhemispherically contrast pattern in the late 1300s, a unique annually resolved ice core record from James Ross Island (*75*), located west of Weddell Sea, depicts unusual cooling remarkably coeval with the strong and warm AMV of the late 1300s (Fig. 4C). The ice core record is strongly correlated with air temperature from nearby weather station (*75*), which is itself correlated with SST of the surrounding seas (fig. S10). Together, the spatial patterns seen in the late 1300s (early 1400s), i.e., extreme precipitation/drought in the tropics (Fig. 5), cooler (warmer) SST anomalies along the U.S. east coast (Fig. 4 and figs. S5 and S8), and cooling (warming) in the southern Atlantic, are all diagnostic of rapid strengthened (weakened) AMOC fingerprint (*6*, *73*, *74*, *76*). These anomalies are also detected during periods of North Atlantic blocking, such as in the 1960s (fig. S8), and they are essentially reversed during the North Atlantic cooling from ~1970s to 1985s (fig. S11) (*74*). This North Atlantic cold period, known as the Great Salinity Anomaly, was concurrent with a weakened AMOC likely induced by increased sea ice export from the Arctic (*56*). These rapid changes are in line with studies showing that abrupt climate events linked with fast AMOC variations are reflected by the interhemispheric SST dipole (*73*, *76*–*78*). Therefore, we speculate that the reconstructed AMOC (Fig. 4B) (*7*), which integrates a network of proxy from around the NH, may be more sensitive to the long-term "global mode" defined by Dima and Lohmann (*73*) and may not efficiently capture the rapid changes involved from the Atlantic mode, such as the two peaks seen in the late 1300s.

The reconstructed AMV illustrates persistent cooling conditions lasting from 1400 until the early 1600s, making it a very long cold period. While we conjecture that the Atlantic water intrusion in the late 1300s was a key driver for the onset of the LIA in the early 1400s, it cannot alone explain a two centuries weakening (cooling) of the SPG as shown in observations and models (*79*, *80*). Other climate feedbacks, principally a sequence of major explosive volcanic eruptions coincident with reductions in emitted solar irradiance, helped to maintain this persistent cooling (*34*, *63*). In brief, this study highlights through observational and paleo evidence that anomalous blocking in the 14th century, linked to extremes in solar activity and low volcanic forcing, led to the intrusion of warm Atlantic water into the Nordic Seas (*51*), which, in turn, resulted in the export of large amounts of ice into the North Atlantic, with downstream effects on the SPG and possibly the AMOC strength. This sequence of events was the precursor to the main phase of the LIA.

MATERIALS AND METHODS

Proxy records

The climate records used in this study were selected on the basis of three criteria: (i) They were characterized by high temporal resolution (<20 years when available); (ii) those in the (sub)Arctic North Atlantic had to be located within the track of the poleward extension of the North Atlantic Current (including the EGC and the Western Greenland Current); and (iii) to reduce the chance of

temporal offset between the different proxies, they had to overlap the period of interest: the transition from the 14th to 15th century with at least one chronological tie point located in the period of interest (see Supplementary Text). The fact that most of them exhibit the two peaks at the end of the 1300s strongly suggests a contemporaneous climatic event.

To investigate the "SST AMOC fingerprint" that is warming in the subpolar region and cooling in the Gulf Stream region (eastern U.S. coast), we used a rare highly resolved record from the Gulf of Maine with annual resolution (*38*). Because the AMV also has linkage with changes in the ITCZ (*20*), we chose climate records known for their sensitivity to ITZC shifts, but again focusing with sufficient temporal resolution (less than <20 years). All the sites are shown in Fig. 1. The solar modulation data (*65*) were linearly interpolated at the annual scale. It is based on absolutely dated tree ring records from England and Switzerland.

Instrumental data

The monthly reconstructed gridded European fields for the 500-hPa geopotential height is based on the area from 80°N to 30°N and 50°W to 40°E on a 2.5 grid (*81*). We then compared our reconstructed AMV with the 500 hPa from the 20th century reanalysis project v3 (*82*) using the same spatial coverage (80°N–30°N and 50°W–40°E) to extend the comparison until 2011. Note that other spatial coverage over the North Atlantic (500 hPa) also revealed strong covariability with our reconstructed AMV (not shown), including the coverage used in (*52*, *56*). For figs. S8 to S11, we used the NOAA (National Oceanic and Atmospheric Administration) Extended SST v5 (*83*), the NCEP/NCAR (National Centers for Environmental Prediction/National Center for Atmospheric Research Reanalysis) was used for the precipitation rate anomaly (*84*), and ERA-Interim reanalysis was used for atmospheric pressure anomaly (*85*). The ISHII data version 6.13 shown in fig. S3 and used in (*71*) is an "AMOC" proxy subsurface temperature and salinity at 24 levels in the upper 1500 m during 1945–2012. It is from M. Ishii and can be obtained at https://rda.ucar.edu/datasets/ds285.3/.

Datasets in the main text

The reconstructed AMV from (*23*) can be obtained at www.ncei.noaa.gov/access/paleo-search/study/31353

North Atlantic Current poleward of 50°N

August temperature in Vøring Plateau off Norway from (*25*) was accessed online on 27 December 2020 at www.ncei.noaa.gov/access/paleo-search/study/17475. Eastern Fram Strait IRD from (*28*) was accessed online on 29 December 2020 at https://doi.pangaea.de/10.1594/PANGAEA.761540. Atlantic water influence based on *C. neoteresis* in Western Fram Strait from (*29*) was accessed online on 5 January 2021 at https://doi.pangaea.de/10.1594/PANGAEA.923844. East Greenland Strait *N. labradorica* from (*30*) was accessed on 27 December 2020 at https://doi.pangaea.de/10.1594/PANGAEA.898355. IRD reported in Denmark Strait from (*32*) was accessed on 28 December 2020 at https://doi.pangaea.de/10.1594/PANGAEA.898363. $\delta^{18}O$ of bivalve shells in the Iceland basin from (*33*) was accessed on 20 December 2020 at www.ncei.noaa.gov/access/paleo-search/study/20448. Sea surface conditions in the Labrador Sea from $\delta^{18}O$ in *N. pachyderma* (red) in site RAPiD-35-COM from (*14*, *18*) were accessed on 15 January 2021 at www.ncei.noaa.gov/access/paleo-search/study/22790. *T. quinqueloba* $\delta^{18}O$ from site RAPiD-35-25B at Eirik Drift from (*18*) was accessed on 17 January 2021 at https://doi.pangaea.de/10.1594/PANGAEA.874286. Data for the percentage of warm water indicators at Disko Bugt, South West Greenland with the individual Atlantic species Melonis barleanus from (*37*) were kindly supplied by D. Wangner. ISOW sortable silt from (*14*) was accessed on 16 February 2021 at www.ncei.noaa.gov/access/paleo-search/study/22790.

AMOC fingerprint

Reconstructed AMOC (*7*) was accessed on 28 June 2021 at www.pik-potsdam.de/~stefan/material/amoc.txt. Reconstructed SST in the Gulf of Maine from bivalve shells (*38*) was accessed on 20 February 2021 at www.ncei.noaa.gov/access/paleo-search/study/6405. Annually resolved δD ice core record from James Ross Island, Antarctica from (*75*) was accessed on 21 May 2021 at www.ncei.noaa.gov/access/paleo-search/study/14201.

The late 1300s as expressed in tropical proxy records

δD at Washington Lake, Central Pacific from (*44*) was accessed on 22 May 2021 at https://www.ncei.noaa.gov/access/paleo-search/study/29432. Huagapo Cave $\delta^{18}O$ in Peru (*46*) was accessed on 7 January 2021 at www.ncei.noaa.gov/access/paleo-search/study/16405. Ice accumulation in meters at Quelccaya Ice Cap, Peru (*47*) was accessed on 22 March 2021 at www.ncei.noaa.gov/pub/data/paleo/icecore/trop/quelccaya/quelccaya2013nd-decadal.txt. $\delta^{18}O$ at Lake Bosumtwi (*48*) was accessed on 24 February 2021 at www.ncei.noaa.gov/access/paleo-search/study/8657.

Atmospheric and solar forcing

The winter (December to February) North Atlantic/European atmospheric pattern from (*81*) was accessed at www.ncei.noaa.gov/access/paleo-search/study/6392. Reconstructed annual solar forcing (*65*) was accessed on 1 February 2021 at www.nature.com/articles/s41561-020-00674-0#Sec16.

Datasets in the Supplementary Materials

SST in the Vøring Plateau from (*26*), as seen in fig. S2, was accessed on 3 January 2021 at https://doi.pangaea.de/10.1594/PANGAEA.820582. Integrated subpolar salinity from (*71*), as seen in fig. S3, was accessed on 5 July 2021 at https://rda.ucar.edu/datasets/ds285.3/. The Chesapeake reconstructed SST from (*39*), as seen in fig. S5, was accessed on 29 August 2021 at www.ncei.noaa.gov/pub/data/paleo/contributions_by_author/cronin2010b/cronin2010b-composite.txt. Titanium concentrations from the Cariaco Basin off Venezuela from (*43*), as seen in fig. S6, were accessed on 8 April 2021 at ftp://ftp.ncdc.noaa.gov/pub/data/paleo/contributions_by_author/haug2001/cariaco_ti.txt. Quelccaya ice core record $\delta^{18}O$ in Peru from (*47*), as seen in fig. S6, was accessed on 17 March 2021 at www.ncei.noaa.gov/access/paleo-search/study/14174

SUPPLEMENTARY MATERIALS

Supplementary material for this article is available at https://science.org/doi/10.1126/sciadv.abi8230

REFERENCES AND NOTES

1. R. S. Bradley, P. D. Jones, 'Little Ice Age' summer temperature variations: Their nature and relevance to recent global warming trends. *The Holocene* **3**, 367–376 (1993).
2. E. Moreno-Chamarro, D. Zanchettin, K. Lohmann, J. H. Jungclaus, Internally generated decadal cold events in the northern North Atlantic and their possible implications for the demise of the Norse settlements in Greenland. *Geophys. Res. Lett.* **42**, 908–915 (2015).
3. A. J. Dugmore, T. H. McGovern, O. Vesteinsson, J. Arneborg, R. Streeter, C. Keller, Cultural adaptation, compounding vulnerabilities and conjunctures in Norse Greenland. *Proc. Natl. Acad. Sci.* **109**, 3658–3663 (2012).
4. W. S. Broecker, D. M. Peteet, D. Rind, Does the ocean–atmosphere system have more than one stable mode of operation? *Nature* **315**, 21–26 (1985).

5. A. J. Broccoli, K. A. Dahl, R. J. Stouffer, Response of the ITCZ to Northern Hemisphere cooling. *Geophys. Res. Lett.* **33**, L01702 (2006).
6. R. Zhang, R. Sutton, G. Danabasoglu, Y. O. Kwon, R. Marsh, S. G. Yeager, D. E. Amrhein, C. M. Little, A review of the role of the Atlantic Meridional Overturning Circulation in Atlantic multidecadal variability and associated climate impacts. *Rev. Geophys.* **57**, 316–375 (2019).
7. S. Rahmstorf, J. E. Box, G. Feulner, M. E. Mann, A. Robinson, S. Rutherford, E. J. Schaffernicht, Exceptional twentieth-century slowdown in Atlantic Ocean overturning circulation. *Nat. Clim. Chang.* **5**, 475–480 (2015).
8. M. S. Lozier, F. Li, S. Bacon, F. Bahr, A. S. Bower, S. A. Cunningham, M. F. de Jong, L. de Steur, B. de Young, J. Fischer, S. F. Gary, B. J. W. Greenan, N. P. Holliday, A. Houk, L. Houpert, M. E. Inall, W. E. Johns, H. L. Johnson, C. Johnson, J. Karstensen, G. Koman, I. A. Le Bras, X. Lin, N. Mackay, D. P. Marshall, H. Mercier, M. Oltmanns, R. S. Pickart, A. L. Ramsey, D. Rayner, F. Straneo, V. Thierry, D. J. Torres, R. G. Williams, C. Wilson, J. Yang, I. Yashayaev, J. Zhao, A sea change in our view of overturning in the subpolar North Atlantic. *Science* **363**, 516–521 (2019).
9. R. T. Sutton, G. D. McCarthy, J. Robson, B. Sinha, A. T. Archibald, L. J. Gray, Atlantic multidecadal variability and the U.K. ACSIS program. *Bull. Am. Meteorol. Soc.* **99**, 415–425 (2018).
10. D. Oldenburg, K. C. Armour, L. Thompson, C. M. Bitz, Distinct mechanisms of ocean heat transport into the Arctic under internal variability and climate change. *Geophys. Res. Lett.* **45**, 7692–7700 (2018).
11. R. Zhang, Coherent surface-subsurface fingerprint of the Atlantic meridional overturning circulation. *Geophys. Res. Lett.* **35**, L20705 (2008).
12. X. Yan, R. Zhang, T. R. Knutson, Underestimated AMOC variability and implications for AMV and predictability in CMIP models. *Geophys. Res. Lett.* **45**, 4319–4328 (2018).
13. L. Caesar, S. Rahmstorf, A. Robinson, G. Feulner, V. Saba, Observed fingerprint of a weakening Atlantic Ocean overturning circulation. *Nature* **556**, 191–196 (2018).
14. P. Moffa-Sánchez, I. R. Hall, North Atlantic variability and its links to European climate over the last 3000 years. *Nat. Commun.* **8**, 1726 (2017).
15. M. W. Miles, C. S. Andresen, C. V. Dylmer, Evidence for extreme export of Arctic sea ice leading the abrupt onset of the Little Ice Age. *Sci. Adv.* **6**, eaba4320 (2020).
16. P. Moffa-Sánchez, I. R. Hall, S. Barker, D. J. Thornalley, I. Yashayaev, Surface changes in the eastern Labrador Sea around the onset of the Little Ice Age. *Paleoceanography* **29**, 160–175 (2014).
17. P. Moffa-Sánchez, E. Moreno-Chamarro, D. J. Reynolds, P. Ortega, L. Cunningham, D. Swingedouw, D. E. Amrhein, J. Halfar, L. Jonkers, J. H. Jungclaus, K. Perner, A. Wanamaker, S. Yeager, Variability in the northern North Atlantic and Arctic oceans across the last two millennia: A review. *Paleoceanogr. Paleoclimatol.* **34**, 1399–1436 (2019).
18. M. Alonso-Garcia, H. K. F. Kleiven, J. F. McManus, P. Moffa-Sanchez, W. S. Broecker, B. P. Flower, Freshening of the Labrador Sea as a trigger for Little Ice Age development. *Clim. Past* **13**, 317–331 (2017).
19. J. R. Knight, C. K. Folland, A. A. Scaife, Climate impacts of the Atlantic multidecadal oscillation. *Geophys. Res. Lett.* **33**, (2006).
20. E. Moreno-Chamarro, J. Marshall, T. Delworth, Linking itcz migrations to the amoc and North Atlantic/pacific sst decadal variability. *J. Clim.* **33**, 893–905 (2020).
21. Y. Asmerom, J. U. L. Baldini, K. M. Prufer, V. J. Polyak, H. E. Ridley, V. V. Aquino, L. M. Baldini, S. F. M. Breitenbach, C. G. Macpherson, D. J. Kennett, Intertropical convergence zone variability in the Neotropics during the Common Era. *Sci. Adv.* **6**, eaax3644 (2020).
22. D. McGee, A. Donohoe, J. Marshall, D. Ferreira, Changes in ITCZ location and cross-equatorial heat transport at the Last Glacial Maximum, Heinrich Stadial 1, and the mid-Holocene. *Earth Planet. Sci. Lett.* **390**, 69–79 (2014).
23. F. Lapointe, R. S. Bradley, P. Francus, N. L. Balascio, M. B. Abbott, J. S. Stoner, G. St-Onge, A. de Coninck, T. Labarre, Annually resolved Atlantic sea surface temperature variability over the past 2,900 y. *Proc. Natl. Acad. Sci.* **117**, 27171–27178 (2020).
24. M. E. Mann, Z. Zhang, S. Rutherford, R. S. Bradley, M. K. Hughes, D. Shindell, C. Ammann, G. Faluvegi, F. Ni, Global signatures and dynamical origins of the Little Ice Age and Medieval Climate Anomaly. *Science* **326**, 1256–1260 (2009).
25. K. Berner, N. Koç, F. Godtliebsen, D. Divine, Holocene climate variability of the Norwegian Atlantic Current during high and low solar insolation forcing. *Paleoceanography* **26**, PA2220 (2011).
26. C. Andersson, B. Risebrobakken, E. Jansen, S. O. Dahl, Late Holocene surface ocean conditions of the Norwegian Sea (Vøring Plateau). *Paleoceanography* **18**, 1044 (2003).
27. R. F. Spielhagen, K. Werner, S. A. Sørensen, K. Zamelczyk, E. Kandiano, G. Budeus, K. Husum, T. M. Marchitto, M. Hald, Enhanced modern heat transfer to the Arctic by warm Atlantic water. *Science* **331**, 450–453 (2011).
28. K. Werner, R. F. Spielhagen, D. Bauch, H. C. Hass, E. Kandiano, K. Zamelczyk, Atlantic Water advection to the eastern Fram Strait—Multiproxy evidence for late Holocene variability. *Palaeogeogr. Palaeoclimatol. Palaeoecol.* **308**, 264–276 (2011).
29. M. Zehnich, R. F. Spielhagen, H. A. Bauch, M. Forwick, H. C. Hass, T. Palme, R. Stein, N. Syring, Environmental variability off NE Greenland (western Fram Strait) during the past 10,600 years. *The Holocene* **30**, 1752–1766 (2020).
30. K. Perner, M. Moros, J. M. Lloyd, E. Jansen, R. Stein, Mid to late holocene strengthening of the East Greenland current linked to warm subsurface atlantic water. *Quat. Sci. Rev.* **129**, 296–307 (2015).
31. S. Funder, A. Jennings, M. Kelly, in *Developments in Quaternary Sciences* (Elsevier, 2004), vol. 2, pp. 425–430.
32. K. Perner, A. E. Jennings, M. Moros, J. T. Andrews, L. Wacker, Interaction between warm Atlantic-sourced waters and the East Greenland Current in northern Denmark Strait (68 N) during the last 10 600 cal a BP. *J. Quat. Sci.* **31**, 472–483 (2016).
33. D. J. Reynolds, J. D. Scourse, P. R. Halloran, A. J. Nederbragt, A. D. Wanamaker, P. G. Butler, C. A. Richardson, J. Heinemeier, J. Eiríksson, K. L. Knudsen, I. R. Hall, Annually resolved North Atlantic marine climate over the last millennium. *Nat. Commun.* **7**, 13502 (2016).
34. G. H. Miller, Á. Geirsdóttir, Y. Zhong, D. J. Larsen, B. L. Otto-Bliesner, M. M. Holland, D. A. Bailey, K. A. Refsnider, S. J. Lehman, J. R. Southon, C. Anderson, H. Björnsson, T. Thordarson, Abrupt onset of the Little Ice Age triggered by volcanism and sustained by sea-ice/ocean feedbacks. *Geophys. Res. Lett.* **39**, L02708 (2012).
35. N. E. Young, A. D. Schweinsberg, J. P. Briner, J. M. Schaefer, Glacier maxima in Baffin Bay during the Medieval Warm Period coeval with Norse settlement. *Sci. Adv.* **1**, e1500806 (2015).
36. M. Wood, E. Rignot, I. Fenty, L. An, A. Bjørk, M. van den Broeke, C. Cai, E. Kane, D. Menemenlis, R. Millan, M. Morlighem, J. Mouginot, B. Noël, B. Scheuchl, I. Velicogna, J. K. Willis, H. Zhang, Ocean forcing drives glacier retreat in Greenland. *Sci. Adv.* **7**, eaba7282 (2021).
37. D. J. Wangner, A. E. Jennings, F. Vermassen, L. M. Dyke, K. A. Hogan, S. Schmidt, K. H. Kjær, M. F. Knudsen, C. S. Andresen, A 2000-year record of ocean influence on Jakobshavn Isbræ calving activity, based on marine sediment cores. *The Holocene* **28**, 1731–1744 (2018).
38. A. D. Wanamaker Jr., K. J. Kreutz, B. R. Schöne, D. S. Introne, Gulf of Maine shells reveal changes in seawater temperature seasonality during the Medieval Climate Anomaly and the Little Ice Age. *Palaeogeogr. Palaeoclimatol. Palaeoecol.* **302**, 43–51 (2011).
39. T. M. Cronin, K. Hayo, R. C. Thunell, G. S. Dwyer, C. Saenger, D. A. Willard, The medieval climate anomaly and little ice age in Chesapeake Bay and the North Atlantic Ocean. *Palaeogeogr. Palaeoclimatol. Palaeoecol.* **297**, 299–310 (2010).
40. A. Newton, R. Thunell, L. Stott, Climate and hydrographic variability in the Indo-Pacific Warm Pool during the last millennium. *Geophys. Res. Lett.* **33**, L19710 (2006).
41. S. J. Langton, B. K. Linsley, R. S. Robinson, Y. Rosenthal, D. W. Oppo, T. I. Eglinton, S. S. Howe, Y. S. Djajadihardja, F. Syamsudin, 3500 yr record of centennial-scale climate variability from the Western Pacific Warm Pool. *Geology* **36**, 795–798 (2008).
42. D. Verschuren, T. C. Johnson, H. J. Kling, D. N. Edgington, P. R. Leavitt, E. T. Brown, M. R. Talbot, R. E. Hecky, History and timing of human impact on Lake Victoria, East Africa. *Proc. R. Soc. Lond. Ser. B Biol. Sci.* **269**, 289–294 (2002).
43. G. H. Haug, K. A. Hughen, D. M. Sigman, L. C. Peterson, U. Röhl, Southward migration of the intertropical convergence zone through the Holocene. *Science* **293**, 1304–1308 (2001).
44. J. P. Sachs, D. Sachse, R. H. Smittenberg, Z. Zhang, D. S. Battisti, S. Golubic, Southward movement of the Pacific intertropical convergence zone AD 1400–1850. *Nat. Geosci.* **2**, 519–525 (2009).
45. D. C. Lund, J. Lynch-Stieglitz, W. B. Curry, Gulf Stream density structure and transport during the past millennium. *Nature* **444**, 601–604 (2006).
46. L. C. Kanner, S. J. Burns, H. Cheng, R. L. Edwards, M. Vuille, High-resolution variability of the South American summer monsoon over the last seven millennia: Insights from a speleothem record from the central Peruvian Andes. *Quat. Sci. Rev.* **75**, 1–10 (2013).
47. L. G. Thompson, E. Mosley-Thompson, M. E. Davis, V. S. Zagorodnov, I. M. Howat, V. N. Mikhalenko, P. N. Lin, Annually resolved ice core records of tropical climate variability over the past ~1800 years. *Science* **340**, 945–950 (2013).
48. T. M. Shanahan, J. T. Overpeckk, J. Anchukaitis, J. W. Beckj, E. Coled, L. Dettman, J. A. Peckc, A. Scholzand, J. W. King, Atlantic forcing of persistent drought in West Africa. *Science* **324**, 377–380 (2009).
49. M. E. Richter, W.-J. von Appen, C. Wekerle, Does the East Greenland current exist in the northern Fram Strait? *Ocean Sci.* **14**, 1147–1165 (2018).
50. T. Kawasaki, H. Hasumi, The inflow ofAtlantic water at theFramStrait and its interannual variability. *J. Geophys. Res. Oceans* **121**, 502–519 (2016).
51. A. Drews, R. J. Greatbatch, Evolution of the Atlantic multidecadal variability in a model with an improved North Atlantic Current. *J. Clim.* **30**, 5491–5512 (2017).
52. S. Häkkinen, P. B. Rhines, D. L. Worthen, Atmospheric blocking and Atlantic multidecadal ocean variability. *Science* **334**, 655–659 (2011).
53. K. Aagaard, E. C. Carmack, The role of sea ice and other fresh water in the Arctic circulation. *J. Geophys. Res. Oceans* **94**, 14485–14498 (1989).

54. L. A. Mysak, S. B. Power, Sea-ice anomalies in the western Arctic and Greenland-Iceland Sea and their relation to an interdecadal climate cycle. *Climatol. Bull.* **26**, 147–176 (1992).
55. H. Wanner, S. Brönnimann, C. Casty, D. Gyalistras, J. Luterbacher, C. Schmutz, D. B. Stephenson, E. Xoplaki, North Atlantic Oscillation—Concepts and studies. *Surv. Geophys.* **22**, 321–381 (2001).
56. M. Ionita, P. Scholz, G. Lohmann, M. Dima, M. Prange, Linkages between atmospheric blocking, sea ice export through Fram Strait and the Atlantic Meridional Overturning Circulation. *Sci. Rep.* **6**, 32881 (2016).
57. C. Kinnard, C. M. Zdanowicz, D. A. Fisher, E. Isaksson, A. de Vernal, L. G. Thompson, Reconstructed changes in Arctic sea ice over the past 1,450 years. *Nature* **479**, 509–512 (2011).
58. C. J. E. Schuurmans, The influence of solar flares on the tropospheric circulation. *The influence of solar flares on the tropospheric circulation* (1969).
59. L. J. Gray, A. A. Scaife, D. M. Mitchell, S. Osprey, S. Ineson, S. Hardiman, N. Butchart, J. Knight, R. Sutton, K. Kodera, A lagged response to the 11 year solar cycle in observed winter Atlantic/European weather patterns. *J. Geophys. Res. Atmos.* **118**, 13405–13420 (2013).
60. L. Gray, T. Woollings, M. Andrews, J. Knight, Eleven-year solar cycle signal in the NAO and Atlantic/European blocking. *Q. J. R. Meteorol. Soc.* **142**, 1890–1903 (2016).
61. D. Barriopedro, R. García-Herrera, R. Huth, Solar modulation of Northern Hemisphere winter blocking. *J. Geophys. Res. Atmos.* **113**, (2008).
62. M. Schwander, M. Rohrer, S. Brönnimann, A. Malik, Influence of solar variability on the occurrence of central European weather types from 1763 to 2009. *Clim. Past* **13**, 1199–1212 (2017).
63. P. Moffa-Sánchez, A. Born, I. R. Hall, D. J. Thornalley, S. Barker, Solar forcing of North Atlantic surface temperature and salinity over the past millennium. *Nat. Geosci.* **7**, 275–278 (2014).
64. Y.-O. Kwon, H. Seo, C. C. Ummenhofer, T. M. Joyce, Impact of multidecadal variability in Atlantic SST on winter atmospheric blocking. *J. Clim.* **33**, 867–892 (2020).
65. N. Brehm, A. Bayliss, M. Christl, H. A. Synal, F. Adolphi, J. Beer, B. Kromer, R. Muscheler, S. K. Solanki, I. Usoskin, N. Bleicher, S. Bollhalder, C. Tyers, L. Wacker, Eleven-year solar cycles over the last millennium revealed by radiocarbon in tree rings. *Nat. Geosci.* **14**, 10–15 (2021).
66. B. S. Barrett, G. R. Henderson, E. McDonnell, M. Henry, T. Mote, Extreme Greenland blocking and high-latitude moisture transport. *Atmos. Sci. Lett.* **21**, e1002 (2020).
67. J. H. Jungclaus, K. Lohmann, D. Zanchettin, Enhanced 20th-century heat transfer to the Arctic simulated in the context of climate variations over the last millennium. *Clim. Past* **10**, 2201–2213 (2014).
68. E. Moreno-Chamarro, D. Zanchettin, K. Lohmann, J. H. Jungclaus, An abrupt weakening of the subpolar gyre as trigger of Little Ice Age-type episodes. *Clim. Dyn.* **48**, 727–744 (2017).
69. I. Yashayaev, Hydrographic changes in the Labrador Sea, 1960–2005. *Prog. Oceanogr.* **73**, 242–276 (2007).
70. D. Oldenburg, R. C. Wills, K. C. Armour, L. Thompson, L. C. Jackson, Mechanisms of low-frequency variability in North Atlantic Ocean heat transport and AMOC. *J. Clim.* **34**, 4733–4755 (2021).
71. X. Chen, K.-K. Tung, Global surface warming enhanced by weak Atlantic overturning circulation. *Nature* **559**, 387–391 (2018).
72. P. Keil, T. Mauritsen, J. Jungclaus, C. Hedemann, D. Olonscheck, R. Ghosh, Multiple drivers of the North Atlantic warming hole. *Nat. Clim. Chang.* **10**, 667–671 (2020).
73. M. Dima, G. Lohmann, Evidence for two distinct modes of large-scale ocean circulation changes over the last century. *J. Clim.* **23**, 5–16 (2010).
74. A. R. Friedman, G. C. Hegerl, A. P. Schurer, S. Y. Lee, W. Kong, W. Cheng, J. C. H. Chiang, Forced and unforced decadal behavior of the interhemispheric SST contrast during the instrumental period (1881–2012): Contextualizing the late 1960s–early 1970s shift. *J. Clim.* **33**, 3487–3509 (2020).
75. N. J. Abram, R. Mulvaney, E. W. Wolff, J. Triest, S. Kipfstuhl, L. D. Trusel, F. Vimeux, L. Fleet, C. Arrowsmith, Acceleration of snow melt in an Antarctic Peninsula ice core during the twentieth century. *Nat. Geosci.* **6**, 404–411 (2013).
76. H. Renssen, H. Goosse, T. Fichefet, Modeling the effect of freshwater pulses on the early Holocene climate: The influence of high-frequency climate variability. *Paleoceanography* **17**, 10-11–10-16 (2002).
77. A. N. LeGrande, G. A. Schmidt, D. T. Shindell, C. V. Field, R. L. Miller, D. M. Koch, G. Faluvegi, G. Hoffmann, Consistent simulations of multiple proxy responses to an abrupt climate change event. *Proc. Natl. Acad. Sci.* **103**, 837–842 (2006).
78. H. Goosse, H. Renssen, F. Selten, R. Haarsma, J. Opsteegh, Potential causes of abrupt climate events: A numerical study with a three-dimensional climate model. *Geophys. Res. Lett.* **29**, 7-1–7-4 (2002).
79. H. Renssen, A. Mairesse, H. Goosse, P. Mathiot, O. Heiri, D. M. Roche, K. H. Nisancioglu, P. J. Valdes, Multiple causes of the Younger Dryas cold period. *Nat. Geosci.* **8**, 946–949 (2015).
80. A. Condron, A. J. Joyce, R. S. Bradley, Arctic sea ice export as a driver of deglacial climate. *Geology* **48**, 395–399 (2020).
81. C. Casty, C. C. Raible, T. F. Stocker, H. Wanner, J. Luterbacher, A European pattern climatology 1766–2000. *Clim. Dyn.* **29**, 791–805 (2007).
82. G. P. Compo, J. S. Whitaker, P. D. Sardeshmukh, Feasibility of a 100-year reanalysis using only surface pressure data. *Bull. Am. Meteorol. Soc.* **87**, 175–190 (2006).
83. B. Huang, P. W. Thorne, V. F. Banzon, T. Boyer, G. Chepurin, J. H. Lawrimore, M. J. Menne, T. M. Smith, R. S. Vose, H. M. Zhang, Extended reconstructed sea surface temperature, version 5 (ERSSTv5): Upgrades, validations, and intercomparisons. *J. Clim.* **30**, 8179–8205 (2017).
84. E. Kalnay, M. Kanamitsu, R. Kistler, W. Collins, D. Deaven, L. Gandin, M. Iredell, S. Saha, G. White, J. Woollen, Y. Zhu, A. Leetmaa, R. Reynolds, M. Chelliah, W. Ebisuzaki, W. Higgins, J. Janowiak, K. C. Mo, C. Ropelewski, J. Wang, R. Jenne, D. Joseph, The NCEP/NCAR 40-year reanalysis project. *Bull. Am. Meteorol. Soc.* **77**, 437–471 (1996).
85. D. P. Dee, S. M. Uppala, A. J. Simmons, P. Berrisford, P. Poli, S. Kobayashi, U. Andrae, M. A. Balmaseda, G. Balsamo, P. Bauer, P. Bechtold, A. C. M. Beljaars, L. van de Berg, J. Bidlot, N. Bormann, C. Delsol, R. Dragani, M. Fuentes, A. J. Geer, L. Haimberger, S. B. Healy, H. Hersbach, E. V. Hólm, L. Isaksen, P. Kållberg, M. Köhler, M. Matricardi, A. P. M. Nally, B. M. Monge-Sanz, J.-J. Morcrette, B.-K. Park, C. Peubey, P. de Rosnay, C. Tavolato, J.-N. Thépaut, F. Vitart, The ERA-Interim reanalysis: Configuration and performance of the data assimilation system. *Q. J. R. Meteorol. Soc.* **137**, 553–597 (2011).

Acknowledgments: We thank the two anonymous reviewers for comments that helped improve this paper. We are grateful to R. Zhang and X. Yan from GFDL/NOAA for help with Fig. 1 and for helpful comments. F.L. is grateful for fruitful discussions with P. Francus and A. Calderhead at INRS, Quebec, E. Thaler at Los Alamos National Lab in New Mexico, and M. Vuille from University at Albany in New York, as well as J. Lapointe from Sentinel North/COPL Laval University, in Quebec. F.L. and R.S.B. are also thankful for productive discussions with L. Ning, Nanjing Normal University. Last but not least, we wish to thank all the research groups for providing public access to their valuable proxy data. **Funding:** We acknowledge support from NSF grant OPP-1744515. **Author contributions:** Conceptualization: F.L. Methodology: F.L. Investigation: F.L. and R.S.B. Visualization: F.L. Supervision: F.L. and R.S.B. Writing, original draft: F.L. and R.S.B. **Competing interests:** The authors declare that they have no competing interests. **Data and materials availability:** All data needed to evaluate the conclusions in the paper are present in the paper, the Supplementary Materials, and the links provided in Materials and Methods.

Submitted 6 April 2021
Accepted 19 October 2021
Published 15 December 2021
10.1126/sciadv.abi8230